



PAPER

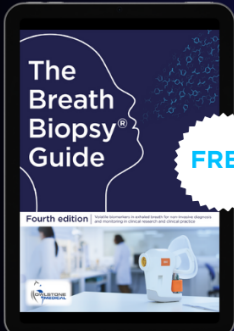
## Evaluation method for the design results of space gravitational-wave telescopes

To cite this article: Jiancong Li *et al* 2023 *Meas. Sci. Technol.* **34** 055409

View the [article online](#) for updates and enhancements.

### You may also like


- [Improvement of image reconstruction in electrical capacitance tomography \(ECT\) by sectorial sensitivity matrix using a K-means clustering algorithm](#)  
P N Darma, M R Baidillah, M W Sifuna et al.
- [Time-domain optics for atomic quantum matter](#)  
Simon Kanthak, Martina Gebbe, Matthias Gersemann et al.
- [Image reconstruction of ECT based on second-order hybrid sensitivity matrix and fuzzy nonlinear programming](#)  
Lifeng Zhang and Da Chen



**FREE** **The Breath Biopsy® Guide**  
Fourth edition

[DOWNLOAD THE FREE E-BOOK](#)

BREATH BIOPSY®



# Evaluation method for the design results of space gravitational-wave telescopes

Jiancong Li<sup>1</sup> , Hongan Lin<sup>1</sup>, Yaozhang Huang<sup>1</sup>, Miao Yu<sup>1</sup>, Jiaxiong Luo<sup>1</sup>, Zihao Xiao<sup>2</sup>, Zhi Wang<sup>3,4,\*</sup> and Yanxiong Wu<sup>1,\*</sup>

<sup>1</sup> School of Physics and Optoelectronic Engineering, Foshan University, Foshan, Guangdong, People's Republic of China

<sup>2</sup> School of Information Science and Engineering, Shandong University, Qingdao, Shandong, People's Republic of China

<sup>3</sup> Changchun Institute of Optics, Fine Mechanics and Physics, Chinese Academy of Sciences, Changchun, People's Republic of China

<sup>4</sup> School of Fundamental Physics and Mathematical Sciences Hangzhou Institute for Advanced Study, UCAS, Hangzhou, People's Republic of China

E-mail: [wz070611@126.com](mailto:wz070611@126.com) and [364477424@qq.com](mailto:364477424@qq.com)

Received 14 July 2022, revised 22 December 2022

Accepted for publication 9 January 2023

Published 17 February 2023



CrossMark

## Abstract

Unlike traditional imaging telescopes, space gravitational-wave telescope has higher requirements for wavefront error and must meet the stability requirement of tilt-to-length (TTL). The tolerance analysis results of current telescopes can judge whether the wavefront error meets the requirements, but they cannot be used as the judgment result of the TTL noise coupling coefficient of the telescope. To analyze the influence of manufacturing errors of the telescope on the coupling coefficient of TTL noise, based on the error amount and the Zernike polynomial first-order sensitivity matrix, we established the sensitivity matrix of the mapping relationship between telescope manufacturing errors and coupling coefficients. For example, consider the design results of an off-axis four-mirror space gravitational-wave telescope. If the wavefront error was used as the judgment result to determine the tolerance distribution, the cumulative probability of the coupling coefficient meeting the requirements would be 66.7%. Furthermore, using the coupling coefficient as the control requirement and determining the tolerance allocation results according to the coupling coefficient sensitivity matrix, the cumulative probability increased to 93.8%. The necessity of using the coupling coefficient as an evaluation method for the design results of gravitational-wave telescopes was verified. This evaluation method can provide meaningful guidance for the design results of gravitational-wave telescopes.

Keywords: space gravitational-wave telescope, coupling coefficient, sensitivity matrix, manufacturing errors

(Some figures may appear in colour only in the online journal)

## 1. Introduction

In February 2016, the ground-based Laser Interferometer Gravitational-Wave Observatory (LIGO) directly detected a gravitational-wave signal generated by the rotation and merger

of two black holes 1.3 billion light-years away. Thus, researchers confirmed and directly measured the predictions of Einstein's general theory of relativity about gravitational waves [1], thereby opening a new chapter in gravitational-wave astronomy. Several gravitational-wave sources in the universe are distributed in the frequency band of 0.1 mHz–1 Hz [2, 3], containing information on the early structure and evolution of the universe, such as that related to double compact star systems,

\* Authors to whom any correspondence should be addressed.

supermassive double black hole orbiting systems, intermediate mass double black hole rotation systems, and supermassive black hole mergers caused by galaxy mergers.

Influenced by the seismic limitation of the Earth's radius, gravity gradient, and anthropogenic noise, among others [4], the detection sensitivity of LIGO is primarily concentrated in the high-frequency band above 1 Hz. To detect gravitational waves in the low-frequency band of 0.1 mHz–1 Hz, Laser Interferometer Space Antenna (LISA), Taiji, and TianQin have been successively proposed. All three interferometers comprise three spacecraft and are equilateral triangular space laser interferometric observatories, with an interference arm having a length in the range of millions of kilometers [5–7]. As the gravitational-wave signal is extremely weak, even if the spacecraft are 3 million km apart, the distance change produced when gravitational waves pass by is approximately 30 pm. This places extremely high demands on a laser interferometry system with a working distance of 3 million km. Compared with the detection of gravitational waves on ground, the detection of gravitational waves in space has obvious advantages in terms of signal strength, the type and quantity of gravitational-wave sources, and the length of the interference arm. The telescope is a subsystem of the space laser interferometry system, which is responsible for measuring the optical path change between the local optical platform and the remote spacecraft optical platform and is essential for the measurement of this ultrahigh-precision displacement. The stability of its optical path length must meet the requirements of  $1 \text{ pm } (\sqrt{\text{Hz}})^{-1}$  [2, 8]. As the spacecraft is easily disturbed by the nonconservative forces in space, the beam received by the telescope is jittered. The wavefront error at the exit pupil of the system is coupled with the tilt-to-length (TTL) noise, which is the second largest noise source in the detection system following shot noise. Currently, the wavefront error of the telescope cannot be eliminated, and the coupling coefficient is required to be lower than  $\pm 25 \text{ pm } \mu\text{rad}^{-1}$  within  $\pm 300 \mu\text{rad}$  of the beam jitter at the exit pupil [9–14].

Space gravitational-wave telescopes have been studied for several years. In accordance with the LISA program, several researchers performed corresponding technical research and experimental verification on telescope materials, dimensional stability, stray-light suppression, and energy transmission efficiency and built a prototype of an off-axis four-mirror telescope [2, 8, 15]. Zhao *et al* conducted a comprehensive theoretical analysis of the influence of telescope aberrations on the TTL-coupled noise and built a prototype telescope for the verification of key technologies of the Taiji program [12, 16]. The wavefront error of the four mirror surfaces in the prototype telescope was 33.5 nm, the overall wavefront error of the system after installation and adjustment was 76 nm, and the maximum coupling coefficient within  $\pm 100 \text{ nrad}$  was  $-3 \text{ pm nrad}^{-1}$ . Upon calculation, the current pointing jitter accuracy was  $10 \text{ nrad } (\sqrt{\text{Hz}})^{-1}$  [17], and the TTL noise of the system was  $30 \text{ pm } (\sqrt{\text{Hz}})^{-1}$ , which no longer met the detection requirements. Unlike traditional imaging telescopes that use wavefront error as a performance evaluation standard,

gravitational-wave telescopes need to meet the requirements of the diffraction limit of wave aberrations and must ensure that the coupling coefficient of the telescope's TTL coupling noise within  $\pm 300 \mu\text{rad}$  of the beam jitter is lower than  $\pm 25 \text{ pm } \mu\text{rad}^{-1}$ . Based on the results of the current tolerance analysis of space gravitational-wave telescopes, it is possible to directly determine whether the wavefront error meets the requirements; however, it is impossible to directly determine whether the coupling coefficient controls the requirements. Therefore, currently, establishing an evaluation method for the coupling coefficient and judging whether the coupling coefficient meets the requirements of gravitational-wave detection are urgent problems to be solved.

The influence of the manufacturing error of the telescope's components on the coupling coefficient must be analyzed. Therefore, in this study, the sensitivity matrix, based on the first-order sensitivity matrix of misalignment and the Zernike polynomial coefficient, was used to map the relationship between the manufacturing error and the coupling coefficient. This sensitivity matrix was established by coupling the wavefront error at the exit pupil of the telescope with the TTL noise. Based on the coupling coefficient's sensitivity matrix, the result of the tolerance analysis of the telescope's optical system was determined, and the wavefront error and coupling coefficient at the exit pupil of the telescope were obtained. To meet the control requirements of space gravitational wave on coupling coefficient, we established the design process of gravitational-wave telescope and introduced the evaluation method of coupling coefficient in the tolerance analysis stage. The design results of the gravitational-wave telescope with a clear aperture of 200 mm and a magnification of 40 were considered as an example. Subsequently, the results of the tolerance of wave aberration or coupling coefficient when they meet the design indicators were, respectively, determined. Additionally, the necessity of using the coupling coefficient as an evaluation method proposed in this study was verified.

## 2. Theoretical analysis

The space laser interferometer receives the measurement beam from the remote spacecraft through the telescope and interferes with the local Gaussian beam on the quadrant photodiode (QPD) after propagation. The phase information was calculated by extracting the complex amplitude of the interference signal. Assuming that the centers of the two interference beams of the flat-top beam  $E_{\text{flat}}$  and Gaussian beam  $E_{\text{gauss}}$  coincide, the complex amplitude is expressed as,

$$O_{\text{ovi}} = \int_S E_{\text{flat}} E_{\text{gauss}}^* \text{d}r^2 = \int_S e^{-\frac{r^2}{\omega(z)^2}} e^{-ikW(r,\theta)} \text{d}r^2, \quad (1)$$

where  $(r, \theta)$  is the polar coordinate above the detector,  $\omega(z)$  is the size of the light spot on the detector, and  $W(r, \theta)$  is the total wavefront error of the system. As Zernike polynomials are orthogonal in the circular domain and correspond to

**Table 1.** Aberrations corresponding to Fringe Zernike polynomials of the first 25 terms.

$A_j^{\text{aber}}$	$z_j(\rho, \theta)$	Aberration name
$A_1^{\text{TI}}$	$2\rho \cos(\theta - \theta_{\text{TI}})$	Tilt (TI)
$A_2^{\text{DE}}$	$\sqrt{3}(2\rho^2 - 1)$	Defocus (DE)
$A_3^{\text{PA}}$	$\sqrt{6}\rho^2 \cos(2\theta - \theta_{\text{PA}})$	Primary astigmatism (PA)
$A_4^{\text{PC}}$	$\sqrt{8}(3\rho^2 - 2\rho) \cos(\theta - \theta_{\text{PC}})$	Primary coma (PC)
$A_5^{\text{PS}}$	$\sqrt{5}(6\rho^4 - 6\rho^2 + 1)$	Primary spherical (PS)
$A_6^{\text{PTR}}$	$\sqrt{8}\rho^3 \cos(3\theta - \theta_{\text{PTR}})$	Primary trefoil (PTR)
$A_7^{\text{SA}}$	$\sqrt{10}(4\rho^4 - 3\rho^2) \cos(2\theta - \theta_{\text{SA}})$	Secondary astigmatism (SA)
$A_8^{\text{SC}}$	$\sqrt{12}(10\rho^5 - 12\rho^3 + 3\rho) \cos(\theta - \theta_{\text{SC}})$	Secondary coma (SC)
$A_9^{\text{SS}}$	$\sqrt{7}(20\rho^6 - 30\rho^4 + 12\rho^2 - 1)$	Secondary spherical (SS)
$A_{10}^{\text{PTE}}$	$\sqrt{10}\rho^4 \cos(4\theta - \theta_{\text{PTE}})$	Primary tetrafoil (PTE)
$A_{11}^{\text{STR}}$	$\sqrt{12}(5\rho^5 - 4\rho^3) \cos(3\theta - \theta_{\text{STR}})$	Secondary trefoil (STR)
$A_{12}^{\text{TA}}$	$\sqrt{14}(15\rho^6 - 20\rho^4 + 6\rho^2) \cos(2\theta - \theta_{\text{TA}})$	Tertiary astigmatism (TA)
$A_{13}^{\text{TC}}$	$4(35\rho^7 - 60\rho^5 + 30\rho^3 - 3\rho) \cos(2\theta - \theta_{\text{TC}})$	Tertiary coma (TC)
$A_{14}^{\text{TS}}$	$3(70\rho^8 - 140\rho^6 + 90\rho^4 - 20\rho^2 + 1)$	Tertiary spherical (TS)

Seidel aberrations, they are often used as the orthogonal basis for wavefront reconstruction. Therefore, the total wavefront error of the system is expressed by the first 25 Fringe Zernike polynomials as,

$$W(\rho, \theta) = \sum_{i=1}^{25} a_i Z_i(\rho, \theta), \quad (2)$$

$$Z_i(\rho, \theta) = \begin{cases} \sqrt{2(n+1)} R_n^m(\rho) \cos(m\theta) & i \text{ is even and } m \neq 0 \\ \sqrt{2(n+1)} R_n^m(\rho) \sin(m\theta) & i \text{ is odd and } m \neq 0, \\ \sqrt{(n+1)} R_n^m & m = 0 \end{cases} \quad (3)$$

$$R_n^m(\rho) = \sum_{s=0}^{n-m} \frac{(-1)^s (n-s)!}{s! \left(\frac{n+m-s}{2}\right)! \left(\frac{n-m-s}{2}\right)!}, \quad (4)$$

where  $R_n^m(\rho)$  are radial polynomials;  $s$ ,  $n$ , and  $m$  are integers; and  $n - m \geq 0$  and  $\rho = r/R$  are normalized radial coordinates. To simplify the following analytical calculation, the cosine and sine terms of the same aberration are combined as follows:

$$a_i Z_i \cos(\theta) + a_{i+1} Z_{i+1} \sin(\theta) = A_j^{\text{aber}} Z_j \cos(\theta - \theta_{\text{aber}}), \quad (5)$$

$$A_j^{\text{aber}} = \sqrt{a_i^2 + a_{i+1}^2}, \theta_{\text{aber}} = \tan^{-1}(a_{i+1}/a_i), \quad (6)$$

where  $A_j^{\text{aber}}$  and  $\theta_{\text{aber}}$  are the amplitude and direction angle of the combined aberration, respectively. The corresponding expression and aberration are given in table 1, where  $A_1^{\text{TI}}$  can be replaced by the pointing jitter angle  $\alpha$ . Therefore, equation (2) can be expressed as follows:

$$W(\rho, \theta) = 2\alpha\rho \cos(\theta - \theta_{\text{TI}}) + \sum_{j=2}^{14} A_j^{\text{aber}} Z_j(\rho, \theta). \quad (7)$$

As the QPD has four integral parts, there are several ways for signal processing. In this paper, by considering the analytical calculation of the LISA Pathfinder (LPF) signal as an example and ignoring the influence of the QPD's slit width on the total amplitude, the phase calculation of the LPF signal can be expressed as,

$$\phi_{\text{LPF}} = \arg \left[ \int_0^1 \rho e^{-\rho^2/\omega_s^2} \left( \int_0^{2\pi} e^{ikW(\rho, \theta)} d\theta \right) d\rho \right]. \quad (8)$$

As we analyzed the effect of the small rotation angle  $\alpha$  on TTL coupled noise, the terms unrelated and higher than the second order of  $\alpha$  were omitted in the analysis. Therefore, the optical path error (OPE) of the system is the ratio of the phase  $\phi_{\text{LPF}}$  obtained from the analysis in equation (8) to the wave number  $k$  (i.e.  $\phi_{\text{LPF}}/k$ ), which is given as,

$$\text{OPE} = B_1 \times \alpha + B_2 \times \alpha^2, \quad (9)$$

$$B_1 = v_1 \times M_1 \times v_2^T, \quad (10)$$

$$B_2 = v_2 \times M_2^T, \quad (11)$$

$$v_1 = [A_4^{\text{PC}}, A_8^{\text{SC}}, A_{13}^{\text{TC}}, A_6^{\text{PTR}}, A_{11}^{\text{STR}}], \quad (12)$$

$$v_2 = [A_2^{\text{DE}}, A_5^{\text{PS}}, A_9^{\text{SS}}, A_{14}^{\text{TS}}, A_3^{\text{PA}}, A_7^{\text{SA}}, A_{12}^{\text{TA}}, A_{10}^{\text{PTE}}], \quad (13)$$

where  $M_1$  and  $M_2$  are the coefficient matrices,  $v_1$  and  $v_2$  are the aberration matrices, and detailed expressions are reflected in the paper [12, 16] and the program [18]. The coupling coefficient  $\delta$  between the TTL noise and the wavefront

error was calculated by the derivation of  $\alpha$  with equation (9) as follows:

$$\delta = B_1 + 2B_2 \times \alpha. \tag{14}$$

Therefore, the coupling coefficient of the gravitational-wave telescope under different wavefront errors can be calculated using equation (14).

### 3. Sensitivity matrix of the coupling coefficient and design process

#### 3.1. Establishing the sensitivity matrix of the coupling coefficient

A traditional imaging telescope usually considers wavefront errors as the evaluation standard in tolerance analysis. However, gravitational-wave telescopes require the system’s wavefront errors to reach the diffraction limit and must calculate the coupling coefficient within  $\pm 300 \mu\text{rad}$  of the beam jitter of less than  $\pm 25 \text{ pm } \mu\text{rad}^{-1}$ . In the tolerance analysis, the change in the wavefront errors of the system can be directly analyzed, but it is difficult to directly determine the change in the coupling coefficient. Therefore, we calculated the change in the coupling coefficient through the influence of manufacturing errors on the amplitude of the Zernike polynomial and equation (14). Assuming that the single error of the telescope’s optical system is small, a first-order linear relationship with the coefficient of the Fringe Zernike polynomial can be observed, which is expressed as follows:

$$\begin{aligned} & \begin{bmatrix} A_1^{\text{TI}}(x + \Delta x_1) & \cdots & A_1^{\text{TI}}(x + \Delta x_n) \\ \vdots & & \vdots \\ A_{14}^{\text{TS}}(x + \Delta x_1) & \cdots & A_{14}^{\text{TS}}(x + \Delta x_n) \end{bmatrix} \\ &= \begin{bmatrix} A_1^{\text{TI}}(x) & \cdots & A_1^{\text{TI}}(x) \\ \vdots & & \vdots \\ A_{14}^{\text{TS}}(x) & \cdots & A_{14}^{\text{TS}}(x) \end{bmatrix} \\ &+ \begin{bmatrix} \frac{\partial A_1^{\text{TI}}(x)}{\partial x} \\ \vdots \\ \frac{\partial A_{14}^{\text{TS}}(x)}{\partial x} \end{bmatrix} \times [\Delta x_1 \quad \cdots \quad \Delta x_n], \end{aligned} \tag{15}$$

where  $\partial A_j^{\text{aber}}/\partial x$  is the sensitivity of the amplitude of the Zernike polynomial under the corresponding error,  $x$  is the initial state of the system, and  $\Delta x_n$  represents the manufacturing errors. Combined with equations (14) and (15), the additional TTL coupling noise caused by the processing and installation errors of a single mirror can be expressed approximately as,

$$\begin{aligned} & \begin{bmatrix} \delta(x + \Delta x_1) - \delta(x) \\ \delta(x + \Delta x_2) - \delta(x) \\ \vdots \\ \delta(x + \Delta x_n) - \delta(x) \end{bmatrix}^T \\ &= \frac{\partial \delta(x)}{\partial x} \times [\Delta x_1 \quad \Delta x_2 \quad \cdots \quad \Delta x_n] \end{aligned} \tag{16}$$

where  $\partial \delta(x)/\partial x$  is the coupling coefficient’s sensitivity of the manufacturing error, and  $\delta(x)$  is the TTL coupling noise under the ideal state of the system. As it is difficult to directly determine the specific relationship between the amplitude of the Zernike polynomial and misalignment in engineering, the difference quotient is usually used to replace the differential quotient. Considering the machining error of the radius of curvature of the primary mirror as an example, the slope obtained by incorporating the influence of the coupling coefficient by several different error values is the sensitivity of the radius of curvature of the primary mirror to the coupling coefficient, which is expressed as,

$$\begin{aligned} & \begin{bmatrix} \delta(R_1 + \Delta R_{1,1}) - \delta(R_1) \\ \delta(R_1 + \Delta R_{1,2}) - \delta(R_1) \\ \vdots \\ \delta(R_1 + \Delta R_{1,n}) - \delta(R_1) \end{bmatrix}^T \\ &= \frac{\Delta \delta(R_1)}{\Delta R_1} \times [\Delta R_{1,1} \quad \Delta R_{1,2} \quad \cdots \quad \Delta R_{1,n}]. \end{aligned} \tag{17}$$

In this study, manufacturing errors of the elements were divided into machining errors and adjustment errors. Machining errors were further divided into curvature radius  $\Delta R$  and conic coefficient  $\Delta k$ , and adjustment errors were divided into rigid-body displacement and inclination. In an off-axis four-mirror optical system, each mirror has six adjustment degrees of freedom, which are the rigid-body displacement  $\Delta d_x$ ,  $\Delta d_y$ , and  $\Delta d_z$  in the  $x$ ,  $y$ , and  $z$  directions and tilt of  $\Delta T_x$ ,  $\Delta T_y$ , and  $\Delta T_z$  around the  $x$ ,  $y$ , and  $z$  axes. The sensitivity of the processing and installation error of a single mirror can be expressed as,

$$\begin{aligned} \frac{\Delta \delta(X_{Mi})}{\Delta X_{Mi}} &= \begin{bmatrix} \frac{\Delta \delta(R_i)}{\Delta R_i} & \frac{\Delta \delta(k_i)}{\Delta k_i} \\ \times \frac{\Delta \delta(d_{xi})}{\Delta d_{xi}} & \frac{\Delta \delta(d_{yi})}{\Delta d_{yi}} & \frac{\Delta \delta(d_{zi})}{\Delta d_{zi}} \\ \times \frac{\Delta \delta(T_{xi})}{\Delta T_{xi}} & \frac{\Delta \delta(T_{yi})}{\Delta T_{yi}} & \frac{\Delta \delta(T_{zi})}{\Delta T_{zi}} \end{bmatrix}. \end{aligned} \tag{18}$$

Therefore, the sensitivity matrix  $S$  of the manufacturing error of the four mirrors  $M_i$  of the telescope’s optical system can be expressed as,

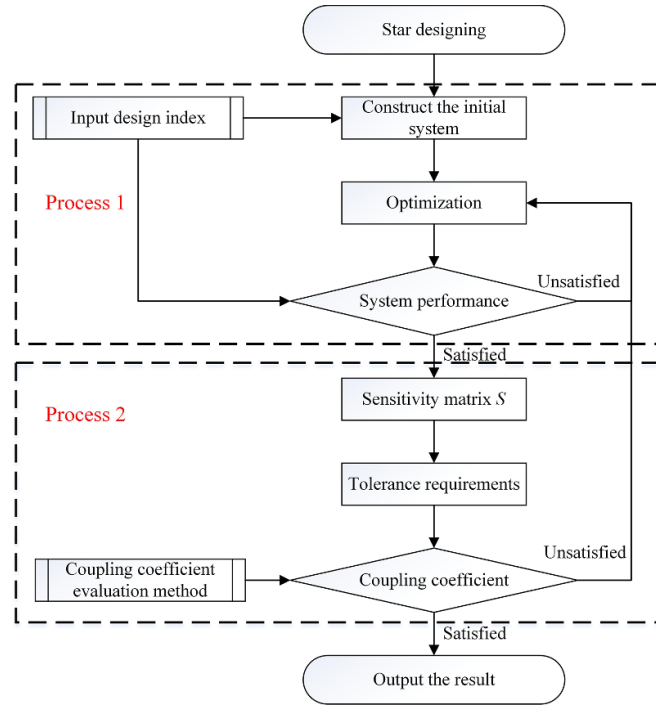


Figure 1. Design flow diagram of the optical system of space gravitational-wave telescopes.

$$S = \begin{bmatrix} \frac{\Delta\delta(X_{M1})}{\Delta X_{M1}} & \frac{\Delta\delta(X_{M2})}{\Delta X_{M2}} & \frac{\Delta\delta(X_{M3})}{\Delta X_{M3}} & \frac{\Delta\delta(X_{M4})}{\Delta X_{M4}} \\ \frac{\Delta\delta(R_1)}{\Delta R_1} & \frac{\Delta\delta(k_1)}{\Delta k_1} & \frac{\Delta\delta(d_{x1})}{\Delta d_{x1}} & \frac{\Delta\delta(d_{y1})}{\Delta d_{y1}} & \frac{\Delta\delta(d_{z1})}{\Delta d_{z1}} & \frac{\Delta\delta(T_{x1})}{\Delta T_{x1}} & \frac{\Delta\delta(T_{y1})}{\Delta T_{y1}} & \frac{\Delta\delta(T_{z1})}{\Delta T_{z1}} \\ \frac{\Delta\delta(R_2)}{\Delta R_2} & \frac{\Delta\delta(k_2)}{\Delta k_2} & \frac{\Delta\delta(d_{x2})}{\Delta d_{x2}} & \frac{\Delta\delta(d_{y2})}{\Delta d_{y2}} & \frac{\Delta\delta(d_{z2})}{\Delta d_{z2}} & \frac{\Delta\delta(T_{x2})}{\Delta T_{x2}} & \frac{\Delta\delta(T_{y2})}{\Delta T_{y2}} & \frac{\Delta\delta(T_{z2})}{\Delta T_{z2}} \\ \frac{\Delta\delta(R_3)}{\Delta R_3} & \frac{\Delta\delta(k_3)}{\Delta k_3} & \frac{\Delta\delta(d_{x3})}{\Delta d_{x3}} & \frac{\Delta\delta(d_{y3})}{\Delta d_{y3}} & \frac{\Delta\delta(d_{z3})}{\Delta d_{z3}} & \frac{\Delta\delta(T_{x3})}{\Delta T_{x3}} & \frac{\Delta\delta(T_{y3})}{\Delta T_{y3}} & \frac{\Delta\delta(T_{z3})}{\Delta T_{z3}} \\ \frac{\Delta\delta(R_4)}{\Delta R_4} & \frac{\Delta\delta(k_4)}{\Delta k_4} & \frac{\Delta\delta(d_{x4})}{\Delta d_{x4}} & \frac{\Delta\delta(d_{y4})}{\Delta d_{y4}} & \frac{\Delta\delta(d_{z4})}{\Delta d_{z4}} & \frac{\Delta\delta(T_{x4})}{\Delta T_{x4}} & \frac{\Delta\delta(T_{y4})}{\Delta T_{y4}} & \frac{\Delta\delta(T_{z4})}{\Delta T_{z4}} \end{bmatrix}^T \quad (19)$$

### 3.2. Design process

Based on the sensitivity matrix of the coupling coefficient proposed in the previous section, the influence of element machining errors, system assembly, and adjustment errors on the coupling coefficient can be judged to determine the result of tolerance allocation. Therefore, combined with the application of the coupling coefficient’s sensitivity matrix in the tolerance analysis, the design process of the optical system of space gravitational-wave telescopes was established, which is primarily divided into two processes, as shown in figure 1.

Process (1): Based on the design requirements of space gravitational-wave telescopes, the initial structure of the off-axis four mirror’s defocused optical path was established. Based on the requirements of the gravitational-wave telescope for magnification, wavefront error, and optical path length stability, the radius of curvature, spacing, and cone coefficient of

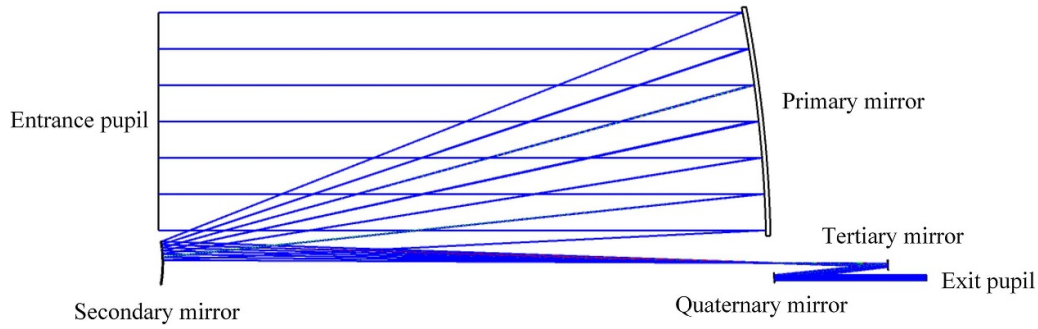
the mirror were optimized as variables. When the design results met the design index requirements, we proceeded to process (2) for analysis.

Process (2): Based on the design results of the space gravitational-wave telescope, the sensitivity matrix of the mapping relationship between the optical element’s manufacturing error and the coupling coefficient was established. The tolerance distribution of the telescope was determined based on the sensitivity matrix of the coupling coefficient. These errors were randomly combined using the Monte Carlo algorithm to evaluate the wavefront error and the coupling coefficient under the corresponding error combination and to estimate the range of variation of the coupling coefficient of the telescope system. If the coupling coefficient meets the requirements of the system index under the tolerance analysis, the results obtained are the final output. Otherwise, the system must be optimized and reevaluated.



**Table 2.** Optical system index of space gravitational-wave telescopes.

Parameter	System requirements
Entrance pupil	200 mm
Wavelength	1064 nm
Field of view (science)	$\pm 8 \mu\text{rad}$
Afocal magnification	40
Wavefront quality over science field of view	$\leq 0.033\lambda$ at 1064 nm
Coupling coefficient	$\leq 25 \text{ pm } \mu\text{rad}^{-1}$

**Figure 2.** Structure of the telescope's optical system.**Table 3.** Design parameters of the telescope's optical system.

Telescope	Radius (m)	Thickness (m)	Conic	Decenter Y (m)	Tilt about X (m)
Primary mirror	-1.214 642	-0.555 535	-1.000 00	-0.130	0
Secondary mirror	-0.114 099	0.677 718	-1.439 70	-0.130	0
Tertiary mirror	-0.497 884	-0.100 000	—	-0.1372	-0.002
Quaternary mirror	0.578 105	0.140 000	—	-0.1397	-0.003 15

#### 4. Design example

To verify the necessity of the proposed evaluation method of the coupling coefficient in the tolerance analysis of space gravitational-wave telescopes, the prototype telescope's design indices of the eLISA or Taiji program were considered as examples for analysis. Table 2 lists the key technical indicators of the gravitational-wave telescope [8, 16]. When the wavefront error at the exit pupil of the telescope is  $0.05\lambda$ , it is adequate to meet the requirements for the Strehl ratio. Therefore, we required the telescope to have a wavefront error of  $0.033\lambda$  to allow for aberrations in the optical bench and to maintain the total system wavefront error at  $0.05\lambda$  or better, with some margin [2]. The system's wavefront quality over the science field of view had a maximum diffraction limit of  $0.033\lambda$  at the exit pupil; furthermore, the coupling coefficient between the system wavefront error and the TTL noise should not exceed  $25 \text{ pm } \mu\text{rad}^{-1}$ .

##### 4.1. Design results and analysis of the telescope

A space gravitational-wave telescope was designed according to the design index requirements of the optical system's design process of space gravitational-wave telescope. The structure of the system is shown in figure 2, and the first imaging plane was located below the primary mirror. The structural parameters

of the four mirrors are listed in table 3. The primary and secondary mirrors were paraboloid and hyperboloid, respectively, and the tertiary and quaternary mirrors were spherical.

The wavefront error at the exit pupil of the full field of view of the telescope was analyzed, and the root-mean-square value of the wavefront error at  $8 \mu\text{rad}$  was the largest and better than  $0.0098\lambda$ , as shown in figure 3(a). The magnitude (Mag) and orientation (Ori) determined using the Fringe Zernike polynomial are listed in table 4. The optical aberration in the wavefront error is represented by the primary astigmatism term  $A_3^{\text{PA}}$ , and the primary coma term  $A_4^{\text{PC}}$  is dominant; the amplitude of higher-order aberrations was small and could be ignored. Figure 3(b) shows the coupling result of the wavefront error with the TTL noise at the exit pupil. Within  $\pm 300 \mu\text{rad}$ , the maximum value of the TTL coupling noise did not exceed  $\pm 2.5 \text{ pm } \mu\text{rad}^{-1}$ , which was lower than the index requirement of  $25 \text{ pm } \mu\text{rad}^{-1}$ .

##### 4.2. Sensitivity matrix analysis of manufacturing errors

Based on the design results of the space gravitational-wave telescope described in the previous section, during the analytical process the machining errors of the radius and conic coefficient, rigid-body displacement, and tilt adjustment errors were applied to the primary, secondary, tertiary, and quaternary mirrors, respectively. The thicknesses of the

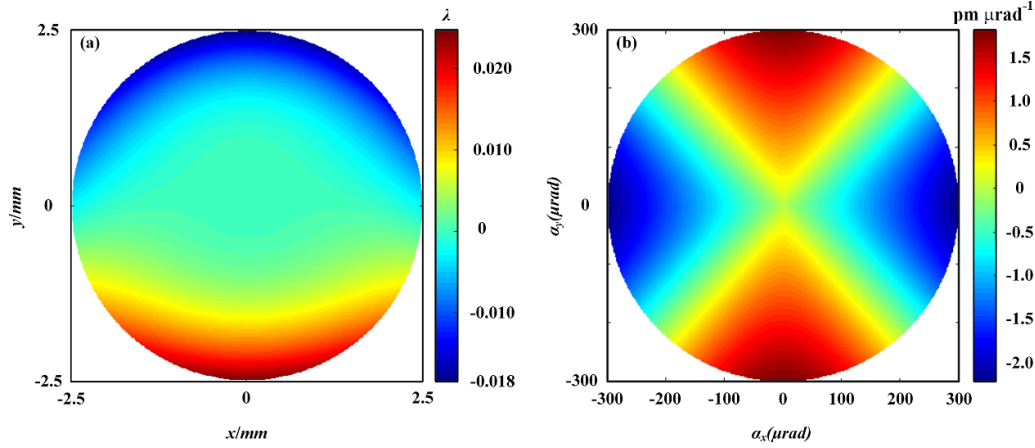


Figure 3. (a) Wavefront at the exit pupil of the telescope after optimization; (b) calculation results of the TTL coupled noise.

Table 4. Amplitude and orientation of the wavefront error at the exit pupil of a telescope based on Zernike polynomials.

Mag/Ori	$A_2^{DE}$	$A_3^{PA}/\theta_{PA}$	$A_4^{PC}/\theta_{PC}$	$A_5^{PS}$	$A_6^{PTR}/\theta_{PTR}$	$A_7^{SA}/\theta_{SA}$	$A_8^{SC}/\theta_{SC}$
nm rad <sup>-1</sup>	0.047	1.56/3.14	3.41/4.71	0.466	0.071/4.71	0.037/3.14	0.010/1.57
Mag/Ori	$A_9^{SS}$	$A_{10}^{PTE}/\theta_{PTE}$	$A_{11}^{STR}/\theta_{STR}$	$A_{12}^{TA}/\theta_{TA}$	$A_{13}^{TC}/\theta_{TC}$	$A_{14}^{TS}$	—
nm rad <sup>-1</sup>	0	0/0	0/0	0/0	0/0	0	—

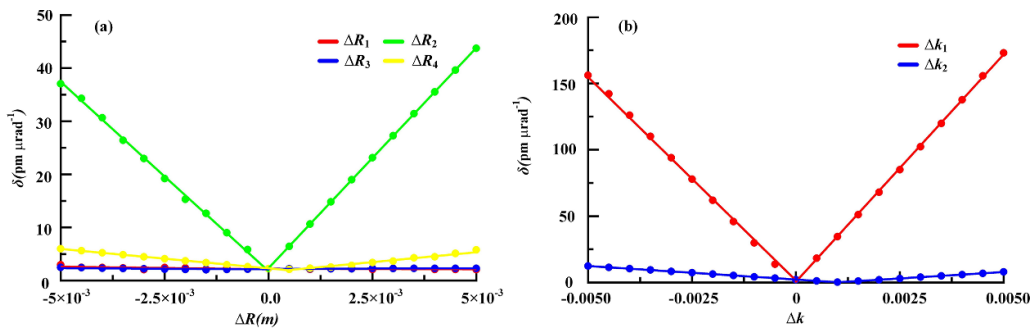


Figure 4. Effect of the machining error on the coupled coefficient. (a) Radius errors; (b) conic *t* errors.

primary and secondary mirrors were used as compensation for optimization.

The sensitivity of each error was fitted by 21 groups of data, and the average value of the slope of the curve fitted in the positive and negative directions was considered as the sensitivity of the error. The results are shown in figures 4 and 5. The influences of machining and adjustment errors on the coupling coefficient were linear. The sensitivity values of the four mirrors are listed in table 5. The results show that the secondary mirror was the most sensitive in the off-axis four-mirror system, and its machining and adjustment errors contributed the most to noise. In the machining error shown in figure 4, the radius of the secondary mirror  $\Delta R_2$  and the conic coefficient of the primary mirror  $\Delta k_1$  had a significant impact on the noise of the system. With the index of 25 pm  $\mu\text{rad}^{-1}$ , the radius error of the secondary mirror  $\Delta R_2$  should be within the range of  $[-3.2 \times 10^{-3}$  to  $2.8 \times 10^{-3}$  m], and the conic coefficient of the primary mirror  $\Delta k_1$  should be within the range of  $[-0.00085$  to  $0.00071]$ . In the adjustment errors shown in figure 5,  $\Delta d_{x2}$ ,  $\Delta d_{y2}$ ,  $\Delta T_{x2}$ , and  $\Delta T_{y2}$  had the

greatest impact. According to the index requirements,  $\Delta d_{x2}$  and  $\Delta d_{y2}$  are required to be in the range of  $[-2.6 \times 10^{-5}$  to  $2.6 \times 10^{-5}$  m] and  $[-2.3 \times 10^{-5}$  to  $2.7 \times 10^{-5}$  m], respectively, and  $\Delta T_{x2}$  and  $\Delta T_{y2}$  are required to be in the range of  $[-93.6''$  to  $110.16'']$  and  $[-105.48''$  to  $105.48'']$ , respectively.

### 4.3. Tolerance analysis of the telescope system

In this section, the tolerance analysis of the design results of space gravitational-wave telescopes is discussed. If the system considers the control requirements of the wavefront error as the final evaluation result, the consequent tolerance distribution results are listed in table 6. A total of 5000 groups of random errors were obtained through the Monte Carlo algorithm. The analysis results of the wavefront error of the optical system corresponding to the manufacturing error are shown in figure 6(a). Furthermore, we calculated the change in the absolute value of the coupling coefficient within  $\pm 300 \mu\text{rad}$  and found that only 66.7% of the cumulative probability was less



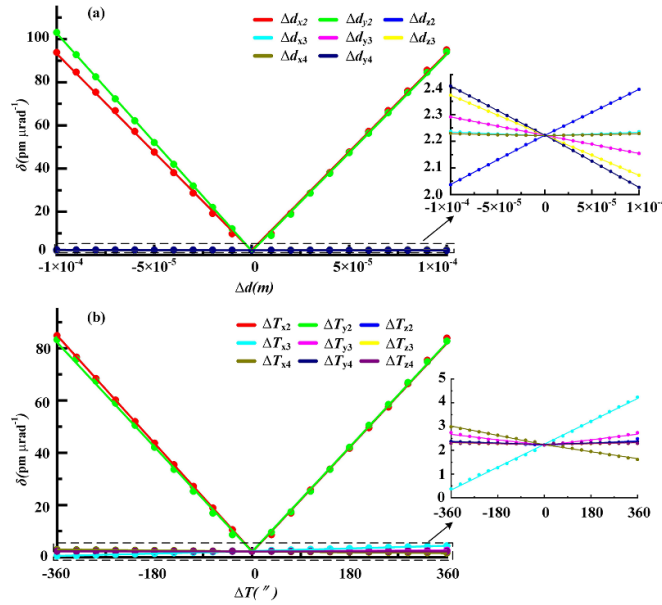


Figure 5. Influence of the adjustment error on the coupling coefficient. (a) Rigid-body displacement error; (b) tilt error.

Table 5. Sensitivity matrix of the coupling coefficient of the telescope’s optical system.

Type	Manufacturing error	Primary mirror	Secondary mirror	Tertiary mirror	Quaternary mirror
Radius	$\Delta R/m$	$1 \times 10^{-5}$	$7.13 \times 10^{-3}$	$3.8 \times 10^{-5}$	$7.46 \times 10^{-4}$
Conic	$\Delta k$	30 623.2	1939.9	—	—
Rigid-body displacement	$\Delta d_x/m$	—	$1.01 \times 10^{-6}$	$1.4 \times 10^{-10}$	0
	$\Delta d_y/m$	—	$9.12 \times 10^{-7}$	$6.8 \times 10^{-10}$	$-1.8 \times 10^{-9}$
	$\Delta d_z/m$	—	$2 \times 10^{-9}$	$1.5 \times 10^{-9}$	—
Tilt	$\Delta T_x/''$	—	0.229	0.0053	0.0021
	$\Delta T_y/''$	—	0.222	0.0013	0.0004
	$\Delta T_z/''$	—	0.0004	0.0002	0.0003

Table 6. Tolerance assignment results with the wavefront error as a control requirement.

Type	Manufacturing error	Primary mirror	Secondary mirror	Tertiary mirror	Quaternary mirror
Radius	$\Delta R/m$	$5 \times 10^{-3}$	$5 \times 10^{-4}$	$5 \times 10^{-3}$	$5 \times 10^{-3}$
Conic	$\Delta k$	0.0005	0.005	—	—
Rigid-body displacement	$\Delta d_x/m$	—	$2 \times 10^{-5}$	$1 \times 10^{-4}$	$1 \times 10^{-4}$
	$\Delta d_y/m$	—	$2 \times 10^{-5}$	$1 \times 10^{-4}$	$1 \times 10^{-4}$
	$\Delta d_z/m$	—	$1 \times 10^{-4}$	$1 \times 10^{-4}$	$1 \times 10^{-4}$
Tilt	$\Delta T_x/''$	—	54	360	360
	$\Delta T_y/''$	—	54	360	360
	$\Delta T_z/''$	—	360	360	360

than  $25 \text{ pm } \mu\text{rad}^{-1}$ , as represented by the red dotted line in figure 6(b).

We considered the control requirement such that the internal coupling coefficient of  $\pm 300 \text{ pm } \mu\text{rad}^{-1}$  was less than  $25 \text{ pm } \mu\text{rad}^{-1}$  as the final evaluation result. In accordance with the sensitivity matrix of the optical system error and coupling coefficient listed in table 5, we further controlled the eccentricity of the secondary mirror in the  $x$  and  $y$  directions, where the coupling coefficient had the greatest influence. We adjusted them from an error value of  $2 \times 10^{-5}$  to  $1.5 \times 10^{-5}$  m, obtained 5000 sets of random errors using the Monte Carlo

algorithm, and calculated the wavefront error and coupling coefficient under the corresponding errors. The tolerance analysis result of the coupling coefficient is shown in figure 7(b). Notably, 93.8% of the cumulative probability was less than  $25 \text{ pm } \mu\text{rad}^{-1}$ , which is a significant improvement in relation to when the system considered the wavefront error control requirement as the final evaluation result. According to the tolerance study of the two cases, even if the wavefront error meets the design index requirement of  $0.033\lambda$ , the coupling coefficient still partially exceeds  $25 \text{ pm } \mu\text{rad}^{-1}$ . Therefore, when the design result of the space gravitational-wave telescope only

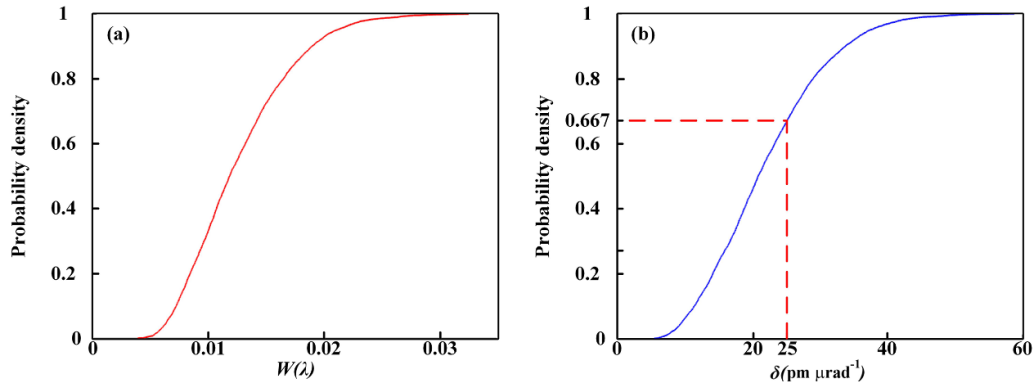


**Figure 6.** Tolerance results when only meeting the requirements of wavefront error. (a) Analysis result of the wavefront error; (b) analysis result of the coupling coefficient.

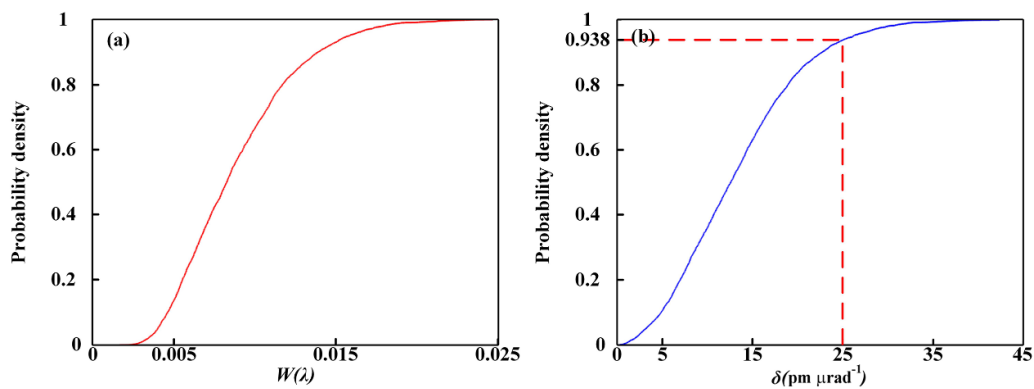


**Figure 7.** Tolerance analysis results when the requirements of coupling coefficient are met. (a) Analysis result of the wavefront error; (b) analysis result of the coupling coefficient.

uses the wave aberration as the final evaluation result, it is insufficient to judge whether it meets the control requirements of optical path length stability.

## 5. Conclusion

In space interferometry system, the telescope is essential for the measurement of this ultrahigh-precision displacement and is the key payload to realize the detection of gravitational waves. To accurately evaluate whether the tolerance analysis results of space gravitational-wave telescope meet the detection requirements, based on the coupling model of the wavefront error and TTL noise, the sensitivity matrix of the mapped relationship between the manufacturing errors of the optical system and coupling coefficients was established. Based on the sensitivity matrix, we proposed an evaluation method for the performance of the telescope's optical system and the design process of space gravitational-wave telescope. To verify the necessity of using the coupling coefficient as an evaluation method, the sensitivity of the mapping relationship between the element error and the coupling coefficient was determined by considering the design results of the off-axis four-mirror afocal optical system as an example. The results indicate that when the wavefront error was used as a control, 66.7% of the cumulative probability of the coupling coefficient was less than 25  $\mu\text{m } \mu\text{rad}^{-1}$  under the corresponding tolerance

distribution. Furthermore, we used the coupling coefficient as the control and determined the tolerance distribution result based on the sensitivity matrix, wherein there was a 93.8% cumulative probability of the coupling coefficient to be less than 25  $\mu\text{m } \mu\text{rad}^{-1}$ . Therefore, when the design results of space gravitational-wave telescopes only consider the wave aberration as the final evaluation result, it is insufficient to judge whether it meets the control requirements of optical path stability. In the tolerance analysis of the design results of the space gravitational-wave telescope, it is necessary to predict and analyze the cumulative probability that the wavefront error reaches the diffraction limit; additionally, the cumulative probability must be evaluated and analyzed such that the coupling coefficient within  $\pm 300 \mu\text{rad}$  is less than 25  $\mu\text{m } \mu\text{rad}^{-1}$  to determine the final tolerance analysis result, which proves that the telescope meets the requirements of space gravitational-wave detection.

## Data availability statement

No new data were created or analyzed in this study.

## Acknowledgments

We acknowledge the financial support from the National Natural Science Foundation of China (No. 62075214), Science

and Technology Plan Project of Guangdong Province (No. X190311UZ190), and research and development projects in key areas of Guangdong Province (No. 2020B1111040001) for funding this research.

### Conflict of interest

The authors declare no conflicts of interest.

### ORCID iD

Jiancong Li  <https://orcid.org/0000-0002-0296-2778>

### References

- [1] Abbott B P *et al* 2016 Observation of gravitational waves from a binary black hole merger *Phys. Rev. Lett.* **116** 061102
- [2] Livas J C and Sankar S R 2016 Optical telescope system-level design considerations for a space-based gravitational wave mission *Proc. SPIE* **9904** 99041K
- [3] Sourath G, Josep S and Guido M 2022 Arm locking performance with the new LISA design *Class. Quantum Grav.* **39** 115009
- [4] Miller M C and Yunes N 2019 The new frontier of gravitational waves *Nature* **568** 469–76
- [5] Karsten D 1996 LISA: laser interferometer space antenna for gravitational wave measurements *Class. Quantum Grav.* **13** A247
- [6] Luo Z, Guo Z K, Jin G, Wu Y and Hu W 2020 A brief analysis to Taiji: science and technology *Results Phys.* **16** 102918
- [7] Luo J *et al* 2016 TianQin: a space-borne gravitational wave detector *Class. Quantum Grav.* **33** 035010
- [8] Sankar S R and Livas J C 2014 Optical telescope design for a space-based gravitational-wave mission *Proc. SPIE* **9143** 914314
- [9] Sasso C P, Mana G and Mottini S 2018 Coupling of wavefront errors and pointing jitter in the LISA interferometer: misalignment of the interfering wavefronts *Class. Quantum Grav.* **35** 245002
- [10] Sankar S R and Livas J C 2020 Optical alignment and wavefront error demonstration of a prototype LISA telescope *Class. Quantum Grav.* **37** 065005
- [11] LISA assessment study report (Yellow Book) 2011 *ESA/SRE 2011* (available at: [https://sci.esa.int/documents/35005/36499/1567258681608-LISA\\_YellowBook\\_ESA-SRE-2011-3\\_Feb2011.pdf](https://sci.esa.int/documents/35005/36499/1567258681608-LISA_YellowBook_ESA-SRE-2011-3_Feb2011.pdf))
- [12] Zhao Y, Shen J, Fang C, Liu H, Wang Z and Luo Z 2020 Tilt-to-length noise coupled by wavefront errors in the interfering beams for the space measurement of gravitational waves *Opt. Express* **28** 25545–61
- [13] Chwalla M *et al* 2016 Design and construction of an optical test bed for LISA imaging systems and tilt-to-length coupling *Class. Quantum Grav.* **33** 245015
- [14] Schuster S, Wanner G, Tröbs M and Heinzel G 2015 Vanishing tilt-to-length coupling for a singular case in two-beam laser interferometers with Gaussian beams *Appl. Opt.* **54** 1010–4
- [15] Livas J C, Arsenovic P, Crow J A, Hill P C, Howard J M, Seals L T and Shiri S 2013 Telescopes for space-based gravitational wave missions *Opt. Eng.* **52** 091811
- [16] Zhao Y, Shen J, Fang C, Wang Z, Gao R and Sha W 2020 The far-field optical path noise coupled with the pointing jitter in the space measurement of gravitational waves *Appl. Opt.* **60** 438–44
- [17] Sasso C P, Mana G and Mottini S 2019 Telescope jitters and phase noise in the LISA interferometer *Opt. Express* **27** 16855–70
- [18] Li J C 2022 Evaluation method for design results of space gravitational wave telescope figshare. Software (<https://doi.org/10.6084/m9.figshare.21687194.v1>)